

**Nonlinear magnetoacoustic waves in rare-earth orthoferrites**

Dmitry L. Dorofeev, Gennady V. Pakhomov, and Boris A. Zon\*

*Mathematical Physics Department, Voronezh State University, Voronezh 394006, Russia*

(Received 13 May 2004; published 18 February 2005)

The dynamics of magnetoacoustic waves in a rare-earth orthoferrite  $\text{YFeO}_3$  crystal is experimentally investigated. The waves are excited by a high-power laser pulse. The analysis of results is carried out taking into account the nonlinear interaction of oscillation modes. It allows us to interpret the results as energy exchange between modes in the time scale, a phenomenon known in nonlinear optics. Based on the proposed model an estimation is obtained for effective nonlinear magnetoacoustic modules of fourth order for yttrium orthoferrite  $\approx 2.5 \times 10^{17} - 2.5 \times 10^{19} \text{J/m}^3$ .

DOI: 10.1103/PhysRevE.71.026607

PACS number(s): 43.25.+y, 72.55.+s

**I. INTRODUCTION**

Magnetoelastic interaction in weak ferromagnetics leads to a giant effective acoustic anharmonicity several orders larger than would be expected in the absence of such interaction. This fact was first noted in work [1] (see also [2]) and experimentally confirmed by observation of acoustic second-harmonic generation and rectification in hematite [3,4] and in thulium orthoferrite in the spin-flip region [5,6].

In the present work acoustic waves were generated using laser excitation of sound, following the technique described in [7,8], which allows one to reach rather high deformations and clearly observe nonlinear processes in a sample, in particular, the changes in time of the energy distribution between different harmonics of magnetization.

A similar phenomenon for progressive electromagnetic waves was theoretically described in nonlinear optics [9,10]. However, in nonlinear acoustics the initial and boundary conditions of the problem, as well as the type of nonlinearity, can be rather different from the ones in optics [11–13]. In particular, in nonlinear optics one usually has only one optical harmonic in the input to the medium, higher harmonics are registered in the output, and the dependence of their intensities on the thickness of the sample is analyzed.

In acoustics, the experiment can be carried out in a completely different way [7,8]: a laser pulse with a duration of several nanoseconds irradiates the surface of a sample giving rise to intensive acoustic oscillations, with excitation of several acoustic modes with different frequencies, and afterward a change of mode amplitudes is observed, due to their nonlinear interaction. In addition, unlike electromagnetic waves, the interacting magnetoacoustic waves are not pure transversal ones but have a mixed transversal-longitudinal character, additionally increasing the complexity of the problem.

In the present paper we discuss this phenomenon of energy exchange between acoustical modes. We interpret it theoretically using the method of effective acoustic anharmonicity [1,2]. This interpretation may be helpful in evaluating effective nonlinear magnetoelastic modules of fourth order.

**II. EXPERIMENTAL SETUP**

We have previously used this method of laser-induced change of magnetization in yttrium orthoferrite [7,8], and its main idea is the following. A pulse of laser radiation gives rise to an initial deformation of the crystal wafer, which then transforms into standing acoustic waves. These acoustic oscillations, due to magnetoelastic and piezomagnetic interactions, lead to changes of magnetization, which can be registered using the induction technique. This technique enables us to register the change of the magnetization component normal to the wafer surface.

Yttrium orthoferrite monocrystals were grown by the technique of crucible-free zone melting. They represented thin plane-parallel wafers cut normally to the [001] axis and normally to the optical axis, with thicknesses  $L = 0.055 - 0.96$  mm and base area  $0.2 - 0.5$  cm<sup>2</sup>.

The wafers were placed in an external magnetic field perpendicular to their plane. The strength of field  $\sim 500$  Oe was sufficient for saturation of magnetization. All the measurements were performed at room temperature. The laser radiation was linearly polarized and had the wavelength  $1.064$   $\mu\text{m}$ , pulse duration  $7 - 15$  ns, and pulse energy  $0.02 - 0.03$  J. The diameter of the laser beam was  $1.5 - 2$  mm.

The magnetization change  $\Delta M$  induced by the laser pulses was registered by a flat coil with diameter of  $3.5$  mm consisting of  $3 - 10$  turns of thin copper wire. The signal from the coil was transmitted after amplification to an oscilloscope. The coil was placed directly on the surface of the sample. The laser beam passed through the central opening of the coil without touching its turns. Such a positional relationship between the wafer and coil allows one to register only the change of magnetic induction in the  $z$  direction, normal to the wafer plane.

The value of the electromotive force from one turn of the coil is proportional to the rate of change of the magnetic induction flux through it:

$$\varepsilon = - \frac{1}{c} \frac{d\Phi}{dt}, \quad \Phi = \int_s (\mathbf{B} \cdot \mathbf{n}) dS, \quad (1)$$

where  $\mathbf{n}$  is the normal to the wafer plane and  $c$  is the light velocity. In Appendix A we give some formulas for calculation of the magnetic induction flux corresponding to a given

\*Electronic address: zon@niif.vsu.ru

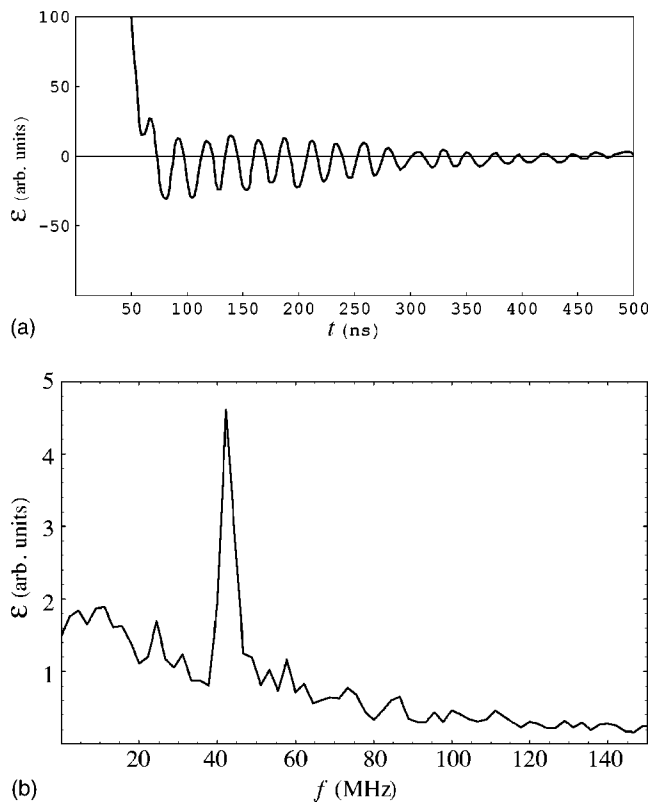


FIG. 1. Magnetoacoustic oscillations in a wafer of thickness 0.088 mm: (a) oscillogram, (b) spectrum. Values on this and following pictures are given in arbitrary units.

distribution of magnetization and some specific cases are considered. Thus, a theoretical calculation of magnetization allows one to find the emf in the coil. Comparing the calculated values with the experimental ones enables us to test the theory developed below of nonlinear magnetoacoustic phenomena in orthoferrites.

### III. EXPERIMENTAL RESULTS

The signal registered by the oscilloscope comprised two parts: an initial pulse, corresponding in form and duration to

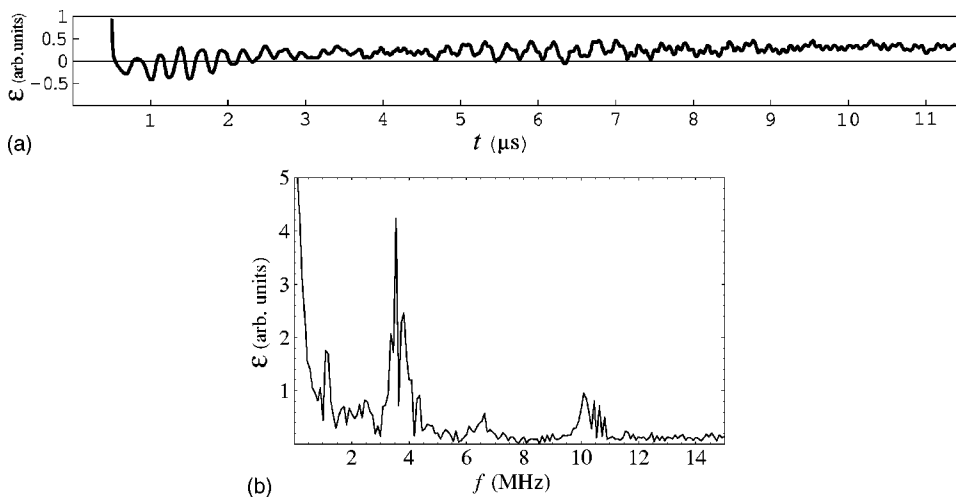


FIG. 2. Magnetoacoustic oscillations in a wafer of thickness 0.58 mm: (a) oscillogram, (b) spectrum.

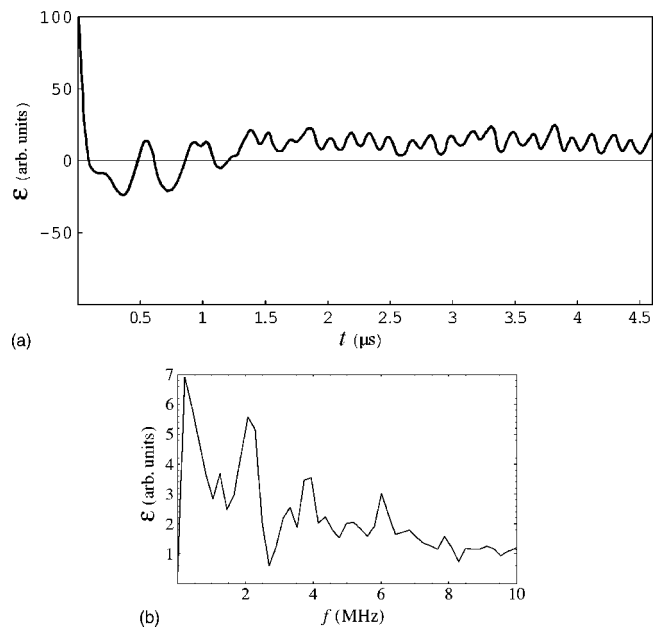


FIG. 3. Magnetoacoustic oscillations in a wafer of thickness 0.96 mm: (a) oscillogram, (b) spectrum.

the initial laser pulse, and an oscillating part, corresponding to a stable sound wave in the wafer. The initial part was analyzed in detail in [7]. In the present work, as well as in [8], we consider the oscillating part.

In experiments we observed three different regimes of oscillations: (i) essentially one-frequency oscillations, observed in thinner plates (Fig. 1); (ii) oscillations with a small number (typically two) of dominating frequencies, observed in plates of intermediate thickness (Fig. 2); (iii) a multiple-frequency regime, observed in thicker plates (Fig. 3).

Figure 1 presents the oscillogram and frequency spectrum of a signal obtained for the wafer with 0.088 mm thickness cut perpendicularly to the axis [001]. As for other thin samples the oscillating part of the signal here has predominantly a single-frequency character. Such a simple structure of the signal is due to the following fact. In this case only the modes with lowest frequencies  $f \approx v/2h$  are excited ( $h$  is the wafer thickness and  $v$  is the velocity of the sound wave in

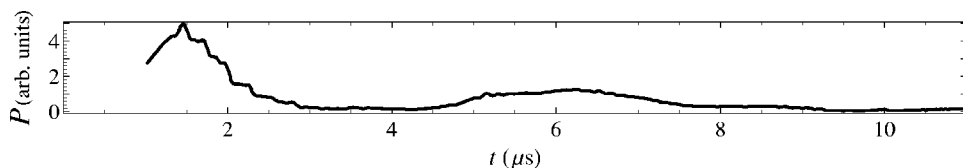


FIG. 4. Intensity of oscillation in the band  $f \approx 3.54 \pm 0.2$  MHz as a function of time for the signal presented in Fig. 2.

the direction perpendicular to the wafer surface), while the modes with higher frequencies  $f \approx vn/2h$ ,  $n=2, 3, \dots$ , are almost absent, because their period for thin samples is much less than the laser pulse duration. The relation  $f \approx v/2h$  enables us to estimate the velocity of the acoustic wave  $v = 2hf$ . For the signal in Fig. 1 we get  $v \approx (7.4 \pm 0.2) \times 10^3$  m/s, which is close to velocity of nearly longitudinal magnetoacoustic eigenwaves along the direction [001] in the YFeO<sub>3</sub> crystal [14–18].

In a thicker sample of  $h=0.58$  mm cut perpendicularly to the optical axis the signal becomes more complex (Fig. 2). It contains mainly the oscillations with frequencies  $f \approx 3.54 \pm 0.2$  MHz, but their third harmonics also have notable amplitudes [see the spectrum in Fig. 2(b)]. Hence in this case not only the lowest oscillation modes arise but also some higher ones. Estimating, from the frequencies of lowest modes, the velocity of the acoustic wave we get  $v \approx (4.1 \pm 0.2) \times 10^3$  m/s, which is close to velocity of nearly transversal magnetoacoustic eigenwaves along the optical axis in the YFeO<sub>3</sub> crystal [14–18].

In a still thicker sample with  $h=0.96$  mm, also cut perpendicularly to the optical axis the signal becomes even more complex (Fig. 3), and its spectrum contains many components with various frequencies. In this case the estimation of wave velocity gives a value  $v \approx (3.8 \pm 0.4) \times 10^3$  m/s, close to the previous one.

With the use of the formulas (1) and expressions given in the Appendixes, it is possible to estimate the magnetization (Appendix A) and corresponding deformation (Appendix B). Thus, for the signal presented in Fig. 2 the amplitude of oscillations of deformation in the oscillating part of the signal was about  $10^{-5}$ – $10^{-4}$ . Such large deformations can induce pronounced nonlinear effects. For comparison it may be noted that second-harmonic generation in orthoferrite near spin flip [5] was observed with deformation  $\sim 10^{-6}$ .

The signal most interesting in this respect is presented in Fig. 2. Its spectrum contains components with various frequencies, but on the other hand it is relatively simple and allows one to interpret it theoretically on a qualitative level of consideration. In particular, it can be inferred that in this case the intensity of oscillations of low mode frequencies  $f \approx 3.54 \pm 0.2$  MHz significantly changes in time: it increases up to the moment  $t \approx 1.5$   $\mu$ s, then it almost disappears, once more increases up to the moment  $t \approx 6$   $\mu$ s, and falls down again.

Such behavior can be described numerically using the sliding window Fourier transformation. The total intensity of oscillations in a frequency band  $f_0 \pm \Delta f$  during a time interval  $t \pm \Delta t$  for a signal  $u(t)$  can be determined as

$$P(t) = \int_{f_0 - \Delta f}^{f_0 + \Delta f} |\bar{u}(t, f)|^2 df, \quad (2)$$

where

$$\bar{u}(t, f) = \int_{t - \Delta t}^{t + \Delta t} u(\tau) e^{-2\pi i f \tau} d\tau. \quad (3)$$

The value of  $\Delta t$  should be sufficiently large in comparison with the period of oscillations at the frequency  $f_0$  and sufficiently small in comparison with the typical time of intensity change. In Fig. 4  $P(t)$  is presented graphically, corresponding to  $f \approx 3.54 \pm 0.2$  MHz and  $\Delta t = 0.5$   $\mu$ s.

This intensity change may be related to energy exchange between oscillation modes due to their nonlinear interaction. In general, such exchange can be both periodic and aperiodic and even chaotic, if the number of interacting modes is large [12]. It must be noted that for the signal presented in Fig. 2 we have not found other frequency bands where intensity would synchronously increase (decrease) in antiphase with its decreases (increases) in the band  $f \approx 3.54 \pm 0.2$  MHz. Nevertheless, this fact does not conflict with the proposed hypothesis of energy exchange between modes, because in the time frame of the experimental technique used we could not observe all oscillation modes but only those generating nonzero magnetization in the direction perpendicular to the sample surface. Thus the observed modes could exchange their energy with some “dark” unobserved modes.

#### IV. THEORY

The general model outlined below describes long-time evolution of coupled stable acoustic waves in a nonlinear anisotropic elastic plate. It is applicable independently to the nature of effective acoustic nonlinearity. With the use of this model one can estimate the modules of effective nonlinear elasticity, which can be difficult to get using other methods.

A quantitative description of experimentally observed oscillation shape variation and dispersion as a function of the plate thickness would be rather desirable, but it could be carried out only on the basis of equally detailed information concerning the values of all nonzero components of the tensors of nonlinear elasticity modules, the magnetoacoustic and piezomagnetic ones. Unfortunately, such information for yttrium orthoferrite is unavailable now. Therefore we are only able so far to develop an idealized general mathematical model of the observed nonlinear magnetoacoustic oscillations, interpret qualitatively the experimental results, and get a rough numeric estimation of the order of magnitude of the effective nonlinear elastic modules of fourth order.

The dependence of displacement field  $\mathbf{U}(\mathbf{r}, t)$  on time is governed by the equation

$$2\rho \frac{\partial^2 U_i}{\partial t^2} = \frac{\partial \sigma_{ij}^{eff}}{\partial x_j}, \quad (4)$$

where  $\rho$  is the density of the crystal,

$$\sigma_{ij}^{eff} = \frac{\partial F_{eff}}{\partial(\partial U_i / \partial x_j)} \quad (5)$$

is the effective strain tensor, determined by the distortion tensor  $\partial U_i / \partial x_j$  and the density of the effective elastic energy of the crystal

$$F_{eff} = C_{ijkl} \frac{\partial U_i}{\partial x_j} \frac{\partial U_k}{\partial x_l} + C'_{ijklmn} \frac{\partial U_i}{\partial x_j} \frac{\partial U_k}{\partial x_l} \frac{\partial U_m}{\partial x_n} + C''_{ijklmnpq} \frac{\partial U_i}{\partial x_j} \frac{\partial U_k}{\partial x_l} \frac{\partial U_m}{\partial x_n} \frac{\partial U_p}{\partial x_q}. \quad (6)$$

The expression (6) has a standard form for the elastic energy of a crystal with inclusion of nonlinear terms. However, when dealing with weak ferromagnetics, the coefficients  $C'$  and  $C''$  are not of purely elastic origin, they effectively take into account the coupling of elastic and magnetic subsystems, as described in [1,2]. Since this coupling is very strong in weak ferromagnetics, the corresponding effective nonlinearities  $C'$  and  $C''$  turn out to be rather high compared with what could be expected in the case of no such coupling. This phenomenon is referred to as giant acoustic anharmonism, and it is comprehensively investigated in [1,2]. The necessity to account in Eq. (6) for not only the third-degree nonlinear terms  $\sim(\partial U_i / \partial x_j)^3$  but also the fourth-degree ones  $\sim(\partial U_i / \partial x_j)^4$  is connected, as will be shown further, with specific peculiarities of the considered problem.

Let us direct the axis  $z$  perpendicularly to the front and back planes of the crystal. The boundary conditions at these free surfaces, i.e., at  $z=0, h$ , have the form

$$\sigma_{iz}^{eff} = 0. \quad (7)$$

Substituting Eqs. (5) and (6) into Eqs. (4) and (7), we get

$$\rho \frac{\partial^2 U_i}{\partial t^2} = 2C_{ijkl} \frac{\partial^2 U_k}{\partial x_j \partial x_l} + 3C'_{ijklmn} \frac{\partial}{\partial x_j} \left[ \frac{\partial U_k}{\partial x_l} \frac{\partial U_m}{\partial x_n} \right] + 4C''_{ijklmnpq} \frac{\partial}{\partial x_j} \left[ \frac{\partial U_k}{\partial x_l} \frac{\partial U_m}{\partial x_n} \frac{\partial U_p}{\partial x_q} \right], \quad (8)$$

$$\left[ 2C_{izkl} \frac{\partial U_k}{\partial x_l} + 3C'_{izklmn} \frac{\partial U_k}{\partial x_l} \frac{\partial U_m}{\partial x_n} + 4C''_{izklmnpq} \frac{\partial U_k}{\partial x_l} \frac{\partial U_m}{\partial x_n} \frac{\partial U_p}{\partial x_q} \right]_{z=0,h} = 0. \quad (9)$$

The transverse size of the crystal plate is much larger than its thickness; hence for the lowest harmonics of the oscillations

$$\frac{\partial U_k}{\partial x}, \frac{\partial U_k}{\partial y} \ll \frac{\partial U_k}{\partial z}.$$

This fact makes it reasonable to omit in Eqs. (8) and (9) all terms that contain differentiation over  $x$  or  $y$ , and hence

$$\rho \frac{\partial^2 U_i}{\partial t^2} = \Gamma_{ij} \frac{\partial^2 U_j}{\partial z^2} + \Gamma'_{ijk} \frac{\partial}{\partial z} \left[ \frac{\partial U_j}{\partial z} \frac{\partial U_k}{\partial z} \right] + \Gamma''_{ijkl} \frac{\partial}{\partial z} \left[ \frac{\partial U_j}{\partial z} \frac{\partial U_k}{\partial z} \frac{\partial U_l}{\partial z} \right], \quad (10)$$

$$\left[ \Gamma_{ij} \frac{\partial U_j}{\partial z} + \Gamma'_{ijk} \frac{\partial U_j}{\partial z} \frac{\partial U_k}{\partial z} + \Gamma''_{ijkl} \frac{\partial U_j}{\partial z} \frac{\partial U_k}{\partial z} \frac{\partial U_l}{\partial z} \right]_{z=0,h} = 0, \quad (11)$$

where

$$\Gamma_{ij} = 2C_{izjz},$$

$$\Gamma'_{ijk} = 3C'_{izjzkz},$$

$$\Gamma''_{ijkl} = 4C''_{izjzkzlz}.$$

One can see that  $\Gamma$  is the Christoffel tensor for the waves propagating along the  $z$  axis;  $\Gamma'$  and  $\Gamma''$  are similar nonlinear tensors.

By means of proper rotation of the coordinate system the Christoffel tensor can be diagonalized:  $\Gamma_{ij} = \rho v^{(i)2} \delta_{ij}$ , where  $v^{(i)}$  are velocities of acoustic eigenwaves. Let us seek the solution of Eq. (10) with boundary conditions (11) in the form of an expansion over these eigenwaves:

$$U_l(z, t) = \sum_{N=-\infty}^{\infty} U_{lN}(t) \cos(k_N z) \exp(i\omega_N^{(l)} t),$$

$$U_{l,-N} = U_{lN}^*, \quad k_N = \frac{\pi N}{h}, \quad \omega_N^{(l)} = k_N v^{(l)}. \quad (12)$$

The above formula for the harmonic frequencies  $\omega_N^{(l)}$  does not account for the frequency dispersion of the sound velocity. To account for this dispersion it is necessary to consider  $v^{(l)}$  as a value depending also upon the index  $N$ .

Substituting Eq. (12) into Eq. (10), we obtain the equations for the amplitudes:

$$\frac{d^2 U_{iQ}}{dt^2} + 2i\omega_Q^{(i)} \frac{dU_{iQ}}{dt} = \sum_{MN} \Gamma'_{ijk} U_{jM} U_{kN} k_M k_N S'_{MNQ} \times \exp[i(\omega_M^{(j)} + \omega_N^{(k)} - \omega_Q^{(i)})t] + \sum_{MNP} \Gamma''_{ijkl} U_{jM} U_{kN} U_{lP} k_M k_N k_P S''_{MNPQ} \times \exp[i(\omega_M^{(j)} + \omega_N^{(k)} + \omega_P^{(l)} - \omega_Q^{(i)})t], \quad (13)$$

where

$$S'_{MNQ} = \frac{2}{h\rho} \int_0^h \cos k_Q z (k_N \cos k_N z \sin k_M z + k_M \cos k_M z \sin k_N z) dz, \quad (14)$$

$$S''_{MNPQ} = -\frac{2}{h\rho} \int_0^h \cos k_Q z (k_N \cos k_N z \sin k_M z \sin k_P z + k_M \cos k_M z \sin k_N z \sin k_P z + k_P \cos k_P z \sin k_M z \sin k_N z) dz. \quad (15)$$

A convenient approach to analyze equations similar to (13) is the averaging technique [19]. Following this approach we assume the amplitudes  $U$  to be slowly changing during

the time interval  $\sim 1/\omega$ , omit the term with the second time derivative in the left-hand side of Eq. (13) and recast these equations maintaining only the slowly varying terms:

$$\begin{aligned}
 2i\omega_Q^{(i)} \frac{dU_{iQ}}{dt} &= \sum_M \Gamma'_{ijk} U_{jM} U_{k,Q-M} k_M k_{Q-M} S'_{M,Q-M,Q} \\
 &\times \exp[i(\omega_M^{(j)} + \omega_{Q-M}^{(k)} - \omega_Q^{(i)})t] \\
 &+ \sum_{MN} \Gamma''_{ijkl} U_{jM} U_{kN} U_{l,Q-M-N} k_M k_N k_{Q-M-N} \\
 &\times S''_{M,N,Q-M-N,Q} \exp[i(\omega_M^{(j)} + \omega_N^{(k)} + \omega_{Q-M-N}^{(l)} \\
 &- \omega_Q^{(i)})t]. \quad (16)
 \end{aligned}$$

It is taken into account here that the eigenwave velocities  $v^{(i)}$  weakly differ; therefore all omitted terms in the right-hand side of Eq. (16) are fast oscillating. Integrating Eq. (14) with  $N=Q-M$  gives us  $S'=0$ . This fact means that the nonlinearity  $\sim (\partial U_i / \partial x_j)^3$  is not essential for the effect under consideration. Such elimination of this nonlinearity is a result of homogeneous boundary conditions of the second kind (7), which arise due to the assumption that the front and back surfaces of the crystal are free. It is well known that such strong dependence of the results on the type of boundary conditions does not take place in linear problems.

Integrating Eq. (15) with  $P=Q-M-N$  gives us

$$S''_{M,N,Q-M-N,Q} = \frac{k_Q}{4\rho}.$$

A detailed analysis of equations similar to (16) was carried out in both nonlinear optics and nonlinear acoustics [9,10,20,21] in the approximation of a finite number of interacting modes. In the present case we get nontrivial results even taking into account only the interaction of first and third harmonics. For a qualitative analysis we neglect below the difference of eigenwave velocities and omit the dependence of all terms upon wave polarization:

$$i \frac{dU_1}{dt} = \frac{3\pi^3 \Gamma''}{8\rho v h^3} U_3 U_1^{*2}, \quad i \frac{dU_3}{dt} = \frac{\pi^3 \Gamma''}{8\rho v h^3} U_1^3. \quad (17)$$

Equations (17) have an integral of motion

$$3|U_3|^2 + |U_1|^2 = \text{const} \equiv A, \quad (18)$$

which presents the acoustic energy conservation law.

Introducing real amplitudes and phases of harmonics

$$U_1 = a_1 e^{i\phi_1}, \quad U_3 = a_3 e^{i\phi_3},$$

let us recast Eqs. (17) as follows:

$$\dot{a}_1 = 3\gamma a_1^2 a_3 \sin \theta,$$

$$\dot{a}_3 = \gamma a_1^3 \sin \theta,$$

$$\dot{\theta} = -\frac{\gamma a_1}{a_3} (a_1^2 - 9a_3^2) \cos \theta, \quad (19)$$

where

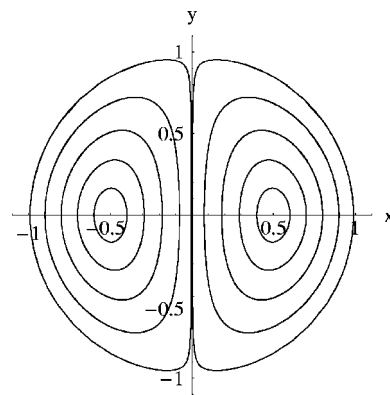


FIG. 5. Phase portrait of system (21):  $x = \rho \cos \theta$ ,  $y = \rho \sin \theta$ ;  $\Delta\rho$  is the distance between a stationary point and the point of the trajectory crossing the  $x$  axis. Trajectories are presented for  $\Delta\rho = 0.1, 0.2, 0.3, 0.4, 0.49$ .

$$\theta = \phi_3 - 3\phi_1, \quad \gamma = \frac{\pi^3 \Gamma''}{8\rho v h^3}.$$

Substituting now the value  $a_1 = \sqrt{A - 3a_3^2}$ , which follows from Eq. (18), into the second and third equations in (19) we get a system of two ordinary differential equations of first order:

$$\dot{a}_3 = \gamma(A - 3a_3^2)^{3/2} \sin \theta,$$

$$\dot{\theta} = -\frac{\gamma(A - 3a_3^2)^{1/2}}{a_3} (A - 12a_3^2) \cos \theta. \quad (20)$$

Transferring to dimensionless variables

$$\rho = \sqrt{3/A} a_3, \quad \tau = A \gamma t,$$

we rewrite these equations in the form

$$\dot{\rho} = -\sqrt{3}(1 - \rho^2)^{3/2} \sin \theta,$$

$$\dot{\theta} = -\sqrt{3} \gamma \frac{(1 - \rho^2)^{1/2}}{\rho} (1 - 4\rho^2) \cos \theta. \quad (21)$$

These equations have stationary points

$$\theta^{(s)} = 0, \pi, \quad \rho^{(s)} = 1/2. \quad (22)$$

Figure 5 presents the phase portrait of this system. One can see that the above stationary points are centers. Phase trajectories close to them are elliptical; further away they become deformed and in the limit transform into unit half circles.

Linearizing Eqs. (21) in the neighborhood of stationary points  $\rho = \rho^{(s)} + \delta\rho$ ,  $\theta = \theta^{(s)} + \delta\theta$ , we readily get that the motion near stationary points has the period (in dimensionless time units  $\tau$ )

$$T_0 = (2/3)^{3/2} \pi \approx 1.71, \quad (23)$$

which is equal (in usual dimensional time units) to

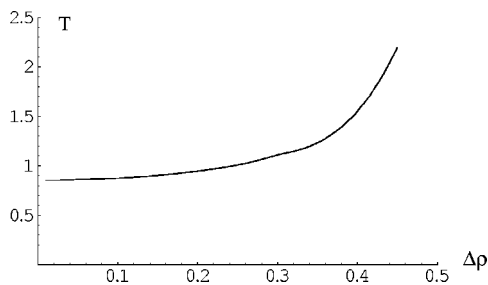


FIG. 6. Period of harmonic exchange  $T$  as a function of  $\Delta\rho$ .

$$T_0 = 1.71 \gamma A. \quad (24)$$

The motion along phase trajectories further from the stationary points becomes slower and tends to infinity at limiting semicircle trajectories (see Fig. 6).

These motions along the phase trajectories represent periodical changes of third-harmonic amplitude  $a_3$ . As follows from the conservation law (18), the first-harmonic amplitude  $a_1$  will also be oscillating with the same frequency, but in antiphase with  $a_3$ . Thus, Eqs. (19) describe the behavior of harmonic amplitudes similar to the one observed in the experiment presented in Fig. 2. In the frame of the proposed model this behavior may be interpreted as an energy exchange between harmonics induced by their nonlinear interaction. It is obvious that in case of a greater number of interacting modes this exchange will be of a more sophisticated aperiodic character similar to the one displayed in Fig. 3.

Substituting into Eq. (24) the experimental values for the typical period of amplitude change  $T \approx 5 \mu\text{s}$  and  $A \approx U^2 \approx 2.5 \times 10^{-19} - 2.5 \times 10^{-17} \text{m}^2$  we get the estimation  $\gamma \approx 5 \times 10^{22} - 5 \times 10^{20}$ , which implies, taking into account Eq. (19),  $\Gamma'' \approx 2.5 \times 10^{19} - 2.5 \times 10^{17} \text{J/m}^3$ . This value agrees with the estimation of corresponding nonlinear elastic modules for hematite  $C_{ijklmnpq} \approx 10^{19} \text{J/m}^3$ , obtained in [1].

Thus the proposed theoretical model satisfactorily explains at a qualitative level the experimentally observed changes of magnetoacoustic mode amplitudes and allows us to estimate the effective nonlinear modules of fourth order for yttrium orthoferrite.

#### ACKNOWLEDGMENTS

We express our gratitude to Professor N. Bloembergen for fruitful notes indicating analogies between nonlinear phenomena in optics and acoustics. We also thank A. Krivchenkova and I. Kretinin for participating in discussion and theoretical analysis of experimental data. The work is carried out with support of CRDF and Ministry of Education of RF (Award No. VZ-010-0).

#### APPENDIX A: CALCULATION OF MAGNETIC INDUCTION FLOW

In order to calculate the induction vector flow through the surface restricted by the contour  $C$ , it is useful to express the induction vector  $\mathbf{B}$  in terms of vector potential  $\mathbf{B} = \text{rot}\mathbf{A}$ , and then the flow may be expressed in terms of circulation

$$\Phi = \int_C \mathbf{A} \cdot d\mathbf{l}. \quad (A1)$$

Thus the calculation of flow becomes reduced to finding the vector potential of the field. Let us suppose that in the region  $V$  there is a stationary magnetization with a continuous distribution  $\mathbf{M}(\mathbf{r})$ . Beyond the region  $V$  the magnetization is equal to zero; therefore at the boundary  $\Gamma$  of  $V$  the magnetization generally undergoes a stepwise discontinuity, a jump from  $\mathbf{M}(\mathbf{r})$  to 0. The vector potential generated by such magnetization has the following form:

$$\mathbf{A}(\mathbf{r}) = \int_V \frac{\text{rot}\mathbf{M}(\mathbf{r}')}{|\mathbf{r} - \mathbf{r}'|} dV' + \int_\Gamma \frac{[\mathbf{n}\mathbf{M}(\mathbf{r}')]_{\Gamma}}{|\mathbf{r} - \mathbf{r}'|} d\Gamma', \quad (A2)$$

where  $\mathbf{n}$  is the outward normal; the integration is carried out over the variable  $\mathbf{r}'$ .

The expressions (A1) and (A2) make it straightforward to find the flow in the case of a static magnetic field. For alternating field these expressions remain valid in the frame of the quasistationary approximation, if the following inequality is satisfied:  $\gamma \ll c/L$ , where  $\gamma$  is a typical frequency of the field,  $c$  is the light velocity, and  $L$  is a typical size of the system (size of region  $V$ , diameter of contour  $C$ , and the distance between them). In the conditions of the discussed experiments this approximation is satisfied with high accuracy.

Let us consider a particular case when the contour  $C$  presents a circle with radius  $R$  located in the plane  $xOy$  with center at the origin, the magnetized region  $V$  is a cylinder of radius  $a$  with the axis coinciding with the coordinate axis  $z$  and upper and lower faces lying at  $z = h_1$  and  $h_2$ , and the magnetization everywhere in  $V$  has a constant value  $\mathbf{M}$ . In this case  $\text{rot}\mathbf{M} = 0$ ; therefore the field is completely determined by the second, surface term in Eq. (A2). Analysis of this term shows that the corresponding flow through the contour  $C$  is equal to the flow generated by a virtual current running along the lateral surface of the cylinder  $V$  with surface density  $cM_z$ . This allows one to write the final expression for the flow in the form

$$\Phi = \eta M_z, \quad \eta \equiv \eta(a, R; h_1, h_2) = c \int_{h_1}^{h_2} L(a, R; z) dz,$$

where

$$L(a, R; z) = \frac{4\pi}{c} \frac{1}{\sqrt{z^2 + (a+R)^2}} \left[ \left( 1 - \frac{k^2}{2} \right) K(k) - E(k) \right],$$

$$k^2 = \frac{4aR}{z^2 + (a+R)^2}$$

is the coefficient of mutual induction for two coaxial ring contours with radii  $R$  and  $a$ , respectively, located at a distance  $z$  one from another [22];  $K$  and  $E$  are full elliptic integrals.

It is obvious that

$$\eta(a, R; h_1, h_2) = \eta(R, a; h_1, h_2),$$

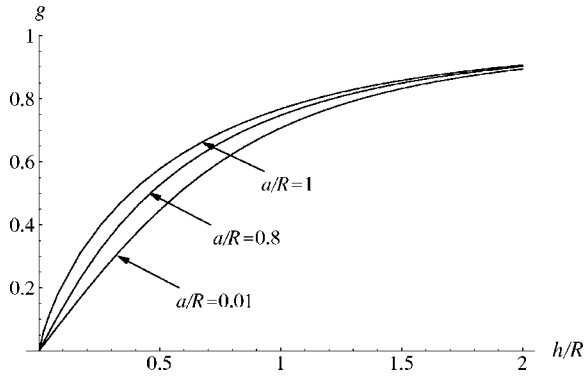


FIG. 7.  $g(a/R; h/R)$  as a function of  $h/R$  for different values of  $a/R$ .

$$\eta(a, R; h_1, h_2) = \eta(R, a; 0, h_2) - \eta(R, a; 0, h_1),$$

$$\eta(R, a; 0, h) = \eta(R, a; -h, 0).$$

Therefore we restrict consideration to  $a \leq R$  and  $h > 0$ . We represent  $\eta(a, R; 0, h)$  as

$$\eta(a, R; 0, h) = 2\pi^2 a^2 g(a/R; h/R), \quad (\text{A3})$$

where the function  $g(a/R; h/R)$  for  $h/R=0-2$  and for some values of  $a/R$  is presented in Fig. 7.

Let us also present some asymptotics.

(1)  $h \ll |R-a|$ ,

$$\eta(a, R; 0, h) \approx chL(a, R; 0).$$

(2)  $h \ll R$  and  $a=R$ ,

$$\eta(a, R; 0, h) \approx 4\pi ah \ln(8a/h).$$

(3)  $h \gg R$  and  $a \leq R$ ,

$$\eta(a, R; 0, h) \approx 2\pi^2 a^2.$$

(4)  $a \ll R$ ,

$$\eta(a, R; 0, h) \approx 2\pi^2 a^2 (h/R) [1 + (h/R)^2]^{-1/2}.$$

Recall that the function  $\eta$  connects the crystal magnetization with the experimentally measured magnetic induction flow.

## APPENDIX B: INTERACTION OF DEFORMATION AND MAGNETIZATION

The orthoferrite  $\text{YFeO}_3$  is antiferromagnetic with weak ferromagnetism. The state of its magnetic system is characterized by the vectors of ferromagnetism  $\mathbf{m} = (\mathbf{M}_1 + \mathbf{M}_2)/2M_0$  and antiferromagnetism  $\mathbf{l} = (\mathbf{M}_1 - \mathbf{M}_2)/2M_0$ , where  $\mathbf{M}_{1,2}$  are the magnetization vectors of sublattices, and  $M_0 = |\mathbf{M}_{1,2}|$  is the saturation magnetization of sublattices. Full magnetization can be presented as  $\mathbf{M} = \mathbf{M}_1 + \mathbf{M}_2 = 2M_0 \mathbf{m}$ . In the case of zero strains the vectors  $\mathbf{l}$  and  $\mathbf{m}$  are directed along crystallographic axes  $a$  and  $c$ , respectively. Under deforma-

tion of the crystal the lengths and directions of these vectors change. This change can be derived from the condition of minimal full energy of the crystal, including pure magnetic, piezomagnetic, and magnetoelastic components [5,7]. We give below final expressions in projections on axes  $a, b$ , and  $c$ :

$$\Delta m_a = \chi_1 \epsilon_{ac},$$

$$\Delta m_b = \chi_2 \epsilon_{bc},$$

$$\Delta m_c = \chi_{31} \epsilon_{aa} + \chi_{32} \epsilon_{bb} + \chi_{33} \epsilon_{cc},$$

$$\Delta l_b = \chi_4 \epsilon_{ab},$$

$$\Delta l_c = \chi_5 \epsilon_{ac},$$

$$\epsilon_{ij} = \frac{1}{2} \left( \frac{\partial U_i}{\partial x_j} + \frac{\partial U_j}{\partial x_i} \right),$$

$$\chi_1 = -\frac{H_D B_{55}}{M_0 H_E H_A},$$

$$\chi_2 = -\frac{\Lambda_{421}}{2M_0 H_E},$$

$$\chi_{3i} = -\frac{\Lambda_{i31}}{4M_0 H_E},$$

$$\chi_4 = -\frac{2B_{66}}{M_0(m_0 H_D - H_A)},$$

$$\chi_5 = -\frac{2B_{55}}{M_0 H_A}.$$

Here  $H_A$  is the field of anisotropy,  $H_E$  is the exchange field,  $H_D$  is the field of Dzyaloshinsky, and  $B, A$  are the magnetoelastic and piezomagnetic modules, respectively. The component  $\Delta l_a$  is set equal to zero, because  $\Delta l_a \ll l_a = l_0$ .

Let us present also the expression for the change of crystal magnetization along the optical axis:

$$\Delta M_z = 2M_0 \Delta m_z = R_1 \epsilon_{yz} + R_2 \epsilon_{zz}, \quad (\text{B1})$$

$$R_1 = 2M_0 \chi_2 \sin \alpha \cos 2\alpha,$$

$$R_2 = 2M_0 (\chi_3 + \chi_2 \sin^2 \alpha) \cos \alpha. \quad (\text{B2})$$

Here the axis  $z$  is directed along the optical axis, the axis  $y$  lies in the plane of crystallographic axes  $b$  and  $c$ , and  $\alpha \approx 52^\circ$  is the angle between the optical axis and the axis  $c$ . The expression (B1) is needed for calculation of the emf with the use of formula (1) for a plate cut perpendicularly to the optical axis.

- [1] V. I. Ozhogin and V. L. Preobrazhenskii, *Sov. Phys. JETP* **46**, 523 (1977).
- [2] V. I. Ozhogin and V. L. Preobrazhenskii, *Sov. Phys. Usp.* **31**, 713 (1988).
- [3] V. N. Ozhogin, A. Yu. Lebedev, and A. Yu. Yakubovski, *JETP Lett.* **27**, 313 (1978).
- [4] V. V. Berezhnov, N. N. Evtikhiev, V. L. Preobrazhenskii, and N. A. Ekonomov *Sov. Phys. Solid State* **24**, 1067 (1982).
- [5] A. Yu. Lebedev, V. I. Ozhogin, V. L. Safonov, and A. Yu. Yakubovskii, *Sov. Phys. JETP* **58**, 616 (1983).
- [6] V. I. Ozhogin and V. L. Preobrazhensky, *J. Magn. Magn. Mater.* **100**, 544 (1991).
- [7] A. M. Balbashov, B. A. Zon, V. Ya. Kupersmidt, G. V. Pakhomov, and T. T. Urazbaev, *Sov. Phys. Solid State* **29**, 743 (1987).
- [8] B. A. Zon and G. V. Pakhomov, *JETP Lett.* **70**, 807 (1999).
- [9] J. A. Armstrong, N. Blombergen, J. Ducuing, and P. S. Pershan, *Phys. Rev.* **127**, 1918 (1962).
- [10] N. Bloembergen, *Nonlinear Optics* (Benjamin, New York, 1965).
- [11] A. F. Kabyshev and V. G. Shargov, *Solid State Phys.* **32**, 2110 (1990).
- [12] V. Preobrazhensky and P. Pernod, *J. Appl. Phys.* **81**, 5709 (1997).
- [13] I. Sh. Akhmadullin, S. A. Migachev, M. F. Sadykov, and M. M. Shakirzyanov, *Phys. Solid State* **46**, 312 (2004).
- [14] Ching H. Tsang, Robert L. White, and Robert M. White, *J. Appl. Phys.* **49**, 1838 (1978).
- [15] Ching H. Tsang, Robert L. White, and Robert M. White, *J. Appl. Phys.* **49**, 6052 (1978).
- [16] M. V. Chetkin, A. I. Akhutkina, N. N. Ermilova, and D. I. Kondratyuk, *Sov. Phys. Solid State* **22**, 1075 (1980).
- [17] M. V. Chetkin, Yu. N. Kurbatova, and A. I. Akhutkina *J. Appl. Phys.* **79**, 6132 (1996).
- [18] A. P. Kuz'menko and V. K. Bulgakov, *Phys. Solid State* **44**, 90 (2002).
- [19] N. N. Bogoliubov and Y. M. Mitropolskii, *Asymptotic Methods in the Theory of Non-linear Oscillations* (Gordon and Breach, New York, 1961).
- [20] O. V. Rudenko and S. I. Soluyan, *Theoretical Foundations of Nonlinear Acoustics* (Plenum, New York, 1977).
- [21] M. B. Vinogradova, O. V. Rudenko, and A. P. Sukhorukov, *Theory of Waves* (Nauka, Moscow, 1990) (in Russian).
- [22] K. Simonyi, *Theoretische Elektrotechnik*, (Ambrosius, Leipzig, Berlin, 1993).